NOTICE
WARNING CONCERNING
COPYRIGHT RESTRICTIONS

Fault tip displacement gradients and process zone dimensions

PATIENCE A. COWIE and ZOE K. SHIPTON

Department of Geology and Geophysics, Edinburgh University, West Mains Road,
Edinburgh EH9 3JW, U.K. E-mail: cowie@glg.ed.ac.uk

Abstract—Finite displacement gradients measured at fault tips appear to contradict the predictions of the post-yield fracture mechanics (PYFM) model for fault tip propagation proposed by Cowie, P. A. and Scholz, C. H. (1992) *Journal of Structural Geology*, **14**, 1133–1148. The results of a high resolution survey of a 3.6 km long normal fault in SE Utah are presented as evidence that the contradiction is real and not simply due to problems of limited resolution. A theoretical explanation for finite tip gradients is then proposed which involves a positive stress feedback between sequential fault slip increments. According to this growth model, strength heterogeneities on a fault surface limit the size of individual ruptures so that only a patch of the fault moves at any one time. Each slipping patch produces a stress perturbation which raises the shear stress on adjacent healed portions of the fault as well as the surrounding rock volume. Healing takes place after each slip event, allowing local strength recovery. Using a simple two-dimensional planar fault model, we show that when the size of the slipping patch is much smaller than the dimensions of the fault plane, and strength recovery is geologically instantaneous, the displacement profile follows an approximately linear decrease towards the tip similar to natural examples. A bell-shaped displacement profile, with tip gradients that tend to zero, is predicted only in the special case where the size of each slip patch equals the fault plane dimensions. Our main modification of the earlier model is that the size of the process zone wake, or frictional breakdown zone, scales with the dimensions of the slipping patch as opposed to the entire fault length. Model results show that the stress field at the tips of faults formed by this mechanism decays rapidly, so the range of significant interaction is small compared to the fault dimensions. © 1998 Elsevier Science Ltd. All rights reserved

INTRODUCTION

The distribution of displacement on faults is a subject that has been discussed at length in recent publications, most notably the relationship between the maximum displacement on a fault and its length (see for example, Walsh and Watterson, 1988; Gillespie *et al.*, 1992; Cowie and Scholz, 1992; Dawers *et al.*, 1993; Cartwright *et al.*, 1995; Schlische *et al.*, 1996; Gross *et al.*, 1997). The aim of this paper is to focus instead on the shape of the displacement profiles and in particular the observed decrease in displacement towards the fault tip line where the displacement, by definition, dies to zero. Understanding the factors which constrain the shape in the tip region provides a basis for extrapolating faults in the subsurface, and is particularly useful in interpreting seismic reflection data where limited resolution poses a major problem in structural analysis (Yielding *et al.*, 1996; Pickering *et al.*, 1997). In this paper, the term *displacement* is used to describe the total accumulated offset that may be measured across a fault, whereas the term *slip* refers to an increment of displacement that occurs in one earthquake (cf. Pollard and Segall, 1987).

Some fault displacement profiles may be qualitatively approximated by the elliptical shape predicted by a simple elastic crack model with uniform loading (Fig. 1). However, stress levels in the surrounding rock implied by such a model are unrealistic, i.e. a stress singularity would exist at the fault tip. The post-yield fracture mechanics (PYFM) model for faults (Cowie and Scholz, 1992), henceforth called C&S92, offered a solution to this problem by including a frictional breakdown zone at the tip which results in a peak stress just equal to the shear strength of the surrounding rock. The latter model is physically more realistic than a purely elastic model, and C&S92 adopted it to predict a linear correlation between maximum displacement and length, controlled by the properties of the rock in which the fault is developing. This prediction has been borne out by subsequent field observations (e.g. Dawers *et al.*, 1993; Schlische *et al.*, 1996; Gross *et al.*, 1997).

However, the profiles predicted by the C&S92 model have a distinctive bell-shape, and the displacement gradient tapers to zero at the fault tip (Fig. 1; see also Burgmann *et al.*, 1994). Some examples of bell-shaped profiles have been observed (e.g. Walsh and Watterson, 1987; Schlische *et al.*, 1996), but an increasing body of data now show that displacement gradients measured in the field appear very often to be significantly greater than zero and approximately constant near the fault tip. This is the case even for isolated fault tips. In fact linear displacement profiles, as illustrated in Fig. 1 and reviewed below, typify isolated faults. Various workers have shown that elastic interaction between neighbouring faults (e.g. Peacock and Sanderson, 1991; Nicol *et al.*, 1996; Willemse *et al.*, 1996), variable frictional properties (Burgmann *et al.*, 1994), and fault propagation rates (Peacock and Sanderson, 1996) do influence the shapes of fault displacement profiles. Although all these factors probably
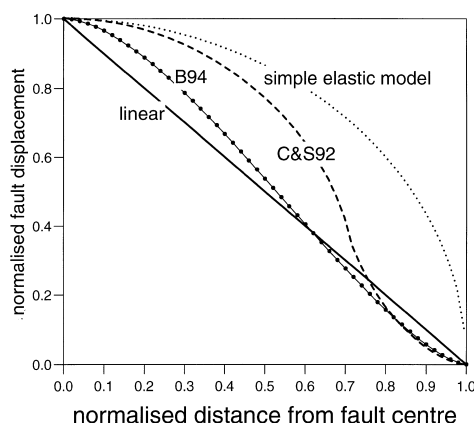
Fig. 1. Comparison of theoretical displacement profiles from the fault centre to the tip, plotted on normalised axes and compared to a linear profile (solid line). Dotted line is elliptical profile predicted by a simple elastic crack model with a constant stress drop; dashed line is PYFM model of Cowie and Scholz (1992) with $\sigma_a/\sigma_o = 0.5$ and $\sigma_f = 0$; line with black dots is calculated assuming a linearly increasing frictional resistance along the whole fault after Burgmann *et al.* (1994).

play an important modifying role, there is no general physical explanation for finite tip displacement gradients which also takes into consideration the requirement for a finite peak stress. The fundamental significance of tip gradient measurements in terms of rock properties is consequently unclear.

C&S92 further argued that the bell-shape of the theoretical displacement profiles could be used to delineate the size, s, of the frictional breakdown zone of the fault. In this zone the surrounding rock is broken down to form a through-going fault surface. According to their model, the transition from the fully developed fault surface into the frictional breakdown zone coincides with the steepest displacement gradient; the length of the tapered portion of the profile is thus a measure of s. The peak stress at the fault tip depends on the ratio s/L as well as D/L, where D is the maximum displacement and L is fault length. Therefore estimating s in the field has potentially important implications for interpreting *in situ* stresses. Scholz *et al.* (1993) and Anders and Wiltschko (1994) presented evidence to suggest that micro-crack damage adjacent to fault surfaces can be related to the parameter s. They refer to this micro-cracking as the process zone wake which is believed to form at the tip as it propagates forward through the rock volume. Vermilye (1996) has since examined several metre-scale faults formed in quartzite to determine how the width, P, of the micro-cracked zone scales with L. She concluded that P is related to L, according to $P \sim 0.01L$. Vermilye (1996) was not able to measure displacement variations along these faults but she argued that the width P is equivalent to the parameter s used by C&S92. The ratio of s/L inferred by C&S92 was approximately 0.15–0.2 which is at least an order of magnitude bigger than that obtained by Vermilye (1996). If s is a significant proportion of L then we would expect tapered displa-

cement profiles for isolated faults to be more generally discernible at the field scale. If $s \ll L$, as suggested by Vermilye (1996), it may be below the resolution of most studies but the resolved part of the profile should then be similar in form to an elliptical shape rather than appearing almost linear (Fig. 1). Assuming a gradual increase in frictional resistance from the centre of the fault to the tips (equivalent to $s = L/2$) produces a profile that is more linear in form, as shown in Fig. 1 (Burgmann *et al.*, 1994). However, near the tips the profile still shows a tapered, i.e. concave upwards, shape not visible in most real fault data. Furthermore, we found no evidence in fault plane exposures to support such a systematic variation in frictional resistance (see Field Study below).

Barr and Houseman (1996) address the tip gradient problem by using a non-linear viscous rheology in contrast to the elastic models described above. Although they are able qualitatively to match finite tip gradients, the main assumptions in their work are that the total accumulated displacement at each point on the fault is proportional to the slip rate and that the fault tip does not propagate. Thus according to these authors the slip rate increases from the tip towards the centre of the fault and the rates are constant with respect to time. This type of model is probably applicable to ductile shear zones where shear velocities are less likely to show large, rapid temporal variations. However, brittle faults generally show 'stick-slip' behaviour and can have low average slip rates which would allow viscous dissipation of tip stresses according to Barr and Houseman's model. If viscous relaxation occurs, then a non-linear displacement–length relationship (i.e. $D = \gamma L^n$, $n > 1$) is predicted which is inconsistent with the majority of observations (see data summary in Schlische *et al.*, 1996).

We present a model for fault growth which is compatible with field observations and the finite-stress rupture criterion for tip propagation implicit in the PYFM model for faulting outlined by C&S92. We show that the field observations can be explained by PYFM theory if frictional healing of the fault surface is taken into account. Healing is a physical and/or chemical process by which a fault recovers its strength, either partially or entirely, after it has ruptured. We argue that the C&S92 model is an end-member solution applicable to the case of a fault that only accumulates displacement during rupture events in which the whole fault area is slipping simultaneously. The other end member, described here, assumes that only patches of the fault slip in any single rupture event and adjacent portions of the fault are healed. We suggest that the latter case is more generally applicable to faults, and is particularly relevant to faults forming in sedimentary rocks which cannot support large elastic strains. A slipping patch model for fault zone development was introduced by Martel and Pollard (1989),

but the implications of healing and repeated rupture have not previously been discussed.

FIELD OBSERVATIONS

Muraoka and Kamata (1983) presented some of the earliest field measurements which clearly showed an approximately linear decrease in displacement towards the tips of metre-scale normal faults formed in a sequence of lacustrine sandstones and shales. Their measurements were taken in the down-dip direction, i.e. the Mode II tips of these faults were exposed. Since then a great deal of data have been compiled from field studies, coal mine plans, and seismic reflection interpretation, primarily from normal faults and usually in plan view (i.e. Mode III fault tips). For example, Walsh and Watterson (1987) compiled a data set of 34 displacement profiles along coalfield normal faults. The average profile through these data shows an approximately linear tip gradient when fault drag is ignored in the displacement measurements. Walsh and Watterson (1987) argued that ductile drag around the faults should be taken into account, in which case they argued a more bell-shaped profile might be expected although it was not verified. Dawers *et al.* (1993) measured fault displacement profiles along normal faults in Owen's Valley California, that ranged in length from 24 m to 182 m, and found that the profiles are best approximated by a triangular shape. For fault lengths ranging from 500 m to 2.2 km the profiles are flat-topped, but the displacement gradients near the tips are approximately constant and of similar magnitude to the smaller-scale faults. Nicol *et al.* (1996) show subsurface displacement data from faults ranging up to several kilometres in length. For the faults they define as isolated, or 'unrestricted', the decrease in displacement from the point of maximum displacement to the tip is remarkably linear (see their fig. 13). Interaction with other faults is shown to modify the profiles so that they differ from the simple triangular shape. Peacock and Sanderson (1996) examined a variety of field data sets and their profile shape for an isolated fault is very similar to that presented by Nicol *et al.* (1996). None of the data these authors present show bell-shaped profiles. Other relevant data come from faults which form in analogue experiments using sand, clay or plaster. These analogue faults show tip displacement profiles very similar to the field examples given here (e.g. Mansfield, 1996).

Field study

It could be argued that the reason bell-shaped profiles, as described by C&S92 and Burgmann *et al.* (1994), are rarely seen is that small displacements near the tips are difficult to detect. From Fig. 1 it is clear that the tapered shape predicted by any of the pro-
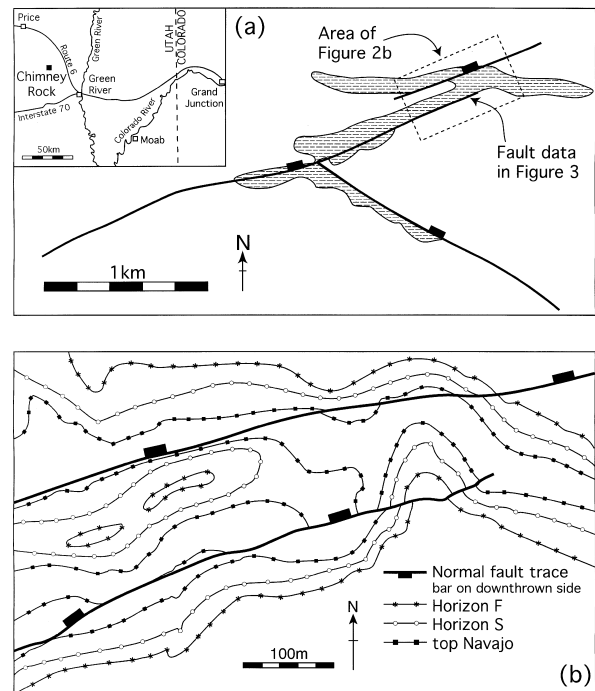

Fig. 2. Normal faults exposed in Jurassic strata in the San Rafael Swell area of SE Utah, U.S.A. (a) Location diagram and sketch map of fault zone studied (modified from Krantz, 1988). Shaded area indicates outcrop of Navajo sandstone. (b) Detailed geology of the fault tip region used to construct the displacement profiles shown in Fig. 3. The fault strikes 076° and dips towards the north at approximately 75°. Slickensides indicate dip-slip motion. Three horizons have been surveyed: the Navajo–Carmel unconformity, and two horizons (F and S) in the lower Carmel Formation.

posed models is most pronounced where the displacement is less than approximately 10–25% of the maximum displacement. In order to investigate this possibility we have mapped in detail the tip region of a 3.6 km long normal fault in SE Utah, U.S.A. (Fig. 2). This fault forms part of the Chimney Rock array in the northern San Rafael Desert which consists of faults ranging in length from 100 m to 6 km, displacing the Navajo Sandstone and overlying Carmel Formation (Krantz, 1988). Erosion of the Carmel in the hanging wall of the faults forms fault-line scarps that run for hundreds of metres. Many faults in the array can be traced for their entire length along strike so that one or both tips are exposed. The plan-view exposure of these faults means that our observations relate to a Mode III fault termination in this case.

The Jurassic Navajo Formation is a well sorted, highly porous aeolian sandstone. Faults formed in this sandstone are surrounded by zones of anastomosing deformation bands. These features are characteristic of deformation in highly porous sandstones and have been extensively studied due to the importance of these rock types as a hydrocarbon reservoirs (Aydin, 1978; Aydin and Johnson, 1978, 1983; Underhill and Woodcock, 1987; Edwards *et al.*, 1993; Antonellini *et al.*, 1994). Positive dilation during shearing of poorly packed grains leads to grain crushing and pore col-

lapse creating a band of fine gouge. This is thought to be a strain hardening process and shear on a single band rapidly becomes inefficient (Antonellini *et al.*, 1994). Deformation is then localised onto the margin of the band, where renewed failure occurs. Continued development leads to the formation of a wide zone of deformation bands and eventually a through-going slip surface forms (Aydin and Johnson, 1978). The faults shown in Fig. 2(b) are clearly defined by polished and striated surfaces in the Navajo sandstone which dip at 65–85° towards the north-northwest. The striations indicate down-dip slip (see also Krantz, 1988). The nature of the striated surfaces shows no systematic lateral variation in character which would be consistent with an increase in frictional resistance towards the fault tip, as proposed by Burgmann *et al.* (1994). The overlying Carmel Formation is a Middle Jurassic thin-bedded limestone. The base of this formation is a regional aerial erosion surface which has gently undulating decimetre-scale topography across the field area. The basal part of the Carmel Formation consists of beds of resistant limestone interspersed with shaley marls. Bedding is laterally continuous and thus provides the marker horizons used to tightly constrain the fault displacement.

The southernmost fault in Fig. 2(b) was mapped in detail to obtain a displacement profile in the tip region (Fig. 3). Some displacement measurements along this fault were compiled by Krantz (1988) and his data from the point of maximum displacement (31 m) to the eastern fault tip are shown in the inset to Fig. 3.

The maximum displacement occurs near the centre of this 3.6 km long fault. Figure 3 shows data from the tip region which has been surveyed up to the point where Krantz's first measurement was obtained. The Navajo–Carmel boundary and marker horizons in the Carmel have been accurately surveyed with a Topcon total station. This is a laser theodolite which gives x, y and z co-ordinates of a reflector positioned at points on the marker horizons. Three surveys, extending up to 500 m behind the fault tip, were amalgamated to give a global set of co-ordinates along the fault zone. These co-ordinates were then used to create accurate geological maps of stratal offsets in the tip area (Fig. 2b). By approximating the Carmel strata as planar layers and using an overall dip of ~4° to the east (averaged from bedding over the entire area of the fault zone), extrapolation of stratum contours allows a stratigraphic separation diagram to be plotted. This allows small variations of dip-slip displacement along the length of the fault to be detected. The resulting tip displacement profile (Fig. 3) shows the separation of the marker horizons down to zero dip-slip offset at the fault tip which is clearly exposed in a canyon. Deformation bands exposed in the canyon walls have only millimetres to centimetres of displacement and do not form a simple continuation of the fault plane.

The total station measures the position of the reflector to ±5 mm precision with a maximum range of 2.5 km. Errors in the displacement profiles introduced during plotting of the maps and stratigraphic separation diagrams are of the order of ±0.5 m vertically
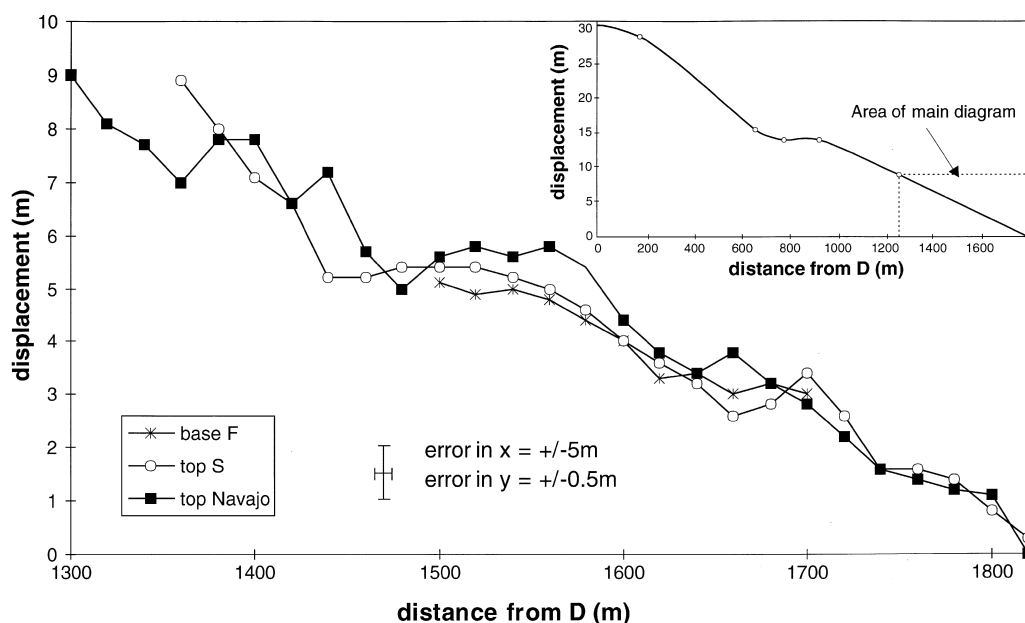

Fig. 3. Displacement profiles in the tip region of the fault indicated in Fig. 2(a), constrained using three stratigraphic marker horizons (see Fig. 2b). Displacement is resolved down to a vertical limit of 0.5 m and the location of the tip is well constrained by good exposure. Inset shows overall displacement profile for the same fault measured by Krantz (1988) from the point of maximum displacement to the eastern fault tip; $L = 3690$ m and $D = 31$ m. The profile is approximately linear up to a distance of about 1 km behind the tip where a north-west trending fault intersects (see Fig. 2a). The average tip displacement gradient is ~0.018 which is very similar to $2(D/L) = 0.017$, i.e. the profile could be approximated by a triangular shape overall.

and ± 5 m horizontally. The assumption of planar bedding around the fault is a simplification but the change in strike between bedding measurements in the foot-wall and hangingwall is small, and does not make a significant impact on the displacement profiles. In other words, deformation of the strata by fault drag or hangingwall roll-over has a negligable effect on the displacement magnitudes along the fault. Finally, the vertical resolution of the measurements is only a few per cent of the maximum fault displacement and thus, according to the models shown in Fig. 1, we should be able to detect any tapering of the profile towards the tip.

It is clear from Fig. 3 that displacement decreases approximately linearly towards the point of zero dip-slip displacement at the tip, similar to what has been found by other workers mentioned above. Even if the deformation bands beyond the tip are included in the profile, the shape does not have the bell-shaped form predicted by C&S92 and Burgmann *et al.* (1994) because the combined displacement is so small (a few centimetres). The three-dimensional geometry of this fault, proximity to neighbouring faults, and rheological contrast between the rock layers are all factors which probably influence the distribution of displacement observed (e.g. Burgmann *et al.*, 1994; Willemse *et al.*, 1996). However, we argue that none of these considerations addresses the problem of how the measured displacement gradient of this individual fault tip is supported by a material of finite strength. The mechanism of displacement accumulation outlined below provides an explanation for this observation. Note that this mechanism is not assumed to be limited to faults forming in high-porosity sandstones, but is generally applicable to the case where faults slip in patches rather than along their entire length and healing is geologically rapid.

CONCEPTUAL FRAMEWORK

The underlying assumption of the C&S92 model is that the total accumulated displacement on a fault may be modelled as if it had been produced in a single slip event affecting the entire present-day length of the fault. Because of this assumption the stress at the fault tip, σ_o, is related in a quantitative way to the maximum accumulated displacement, D, the remote stress, σ_a, the frictional resistance on the fault, σ_f, and the fault length, L. The size of the frictional breakdown zone, s, is predicted to scale linearly with L if σ_o, σ_a and σ_f are independent of L. This result is a consequence of the model formulation which imposes a constant stress drop ($\sigma_a - \sigma_f$) over the entire length, L, and an excess frictional resistance ($\sigma_o - \sigma_f$), over the distance s; the ratio of these stress differences controls the value of D. Because σ_o and σ_f are material properties and σ_a is a function of the tectonic setting, self-similar growth

is predicted, i.e. D scales linearly with L. If a fault only accumulates displacement in slip events with a rupture length equal to L, and the fault does not move at all between slip events, then the underlying assumption of the C&S92 model may be justified. In other words, the net effect of a sequence of increments in which the entire fault surface slips simultaneously may be modelled as a single increment if the material in which the fault forms behaves in a linear elastic fashion.

An alternative scenario is that only a portion of the fault moves at any given time and adjacent healed sections of the fault, as well as the surrounding rock volume, can support the stress changes around the slipped patch. This has two important consequences: the rock volume surrounding the tip is less stressed than if the entire fault plane slips, and secondly the fault itself is now reloaded along co-planar healed sections and brought closer to failure than would be the case if only regional tectonic loading was applied. We may still impose the restriction that the peak stress at the tip of the fault (or of an individual rupture) is finite, limited by the local rock strength (or frictional resistance). However, now we have the case that the parameter s scales with the size of the slipped patch, R, where $R \leq L$. If the slipped patch recovers its strength by healing before future ruptures occur then the process can be repeated. The C&S92 model is the end-member case where $R = L$ and s then scales with L. The other end-member occurs if $R \ll L$ so that s becomes very small. Note that in this case the parameters σ_o, σ_a and σ_f defined by C&S92 now refer to slip on a pre-existing fault surface rather than a fault growing through intact rock. Observations show that some faults clearly do move in major earthquakes while others appear to creep stably or move in smaller magnitude seismic events. These two processes are unlikely to be mutually exclusive, but an important question is whether the same long-term displacement profiles are produced if one of these two mechanisms dominates.

Figure 4 illustrates the mechanism proposed here for the case of a normal fault. The slipping patch represents movement on the fault during one discrete slip event, e.g. a single earthquake, while the rest of the fault surface does not move. The stress perturbation due to the slipping patch is shown in Fig. 4(b), indicating regions where the stress level is raised ($+$) or lowered ($-$) on planes that are co-planar with or parallel to the rupture plane. The magnitude and sign of the stress perturbation is a function of normal and shear stress changes induced by the rupture. The combined effect is called the 'Coulomb stress change' (King *et al.*, 1994) and is shown here for rupture on a fault dipping at $60°$ (modified from Hodgkinson *et al.*, 1996). Note that the fault plane along-strike from the slipping patch feels an increased stress level and the stress perturbation decays with distance from the ends of the
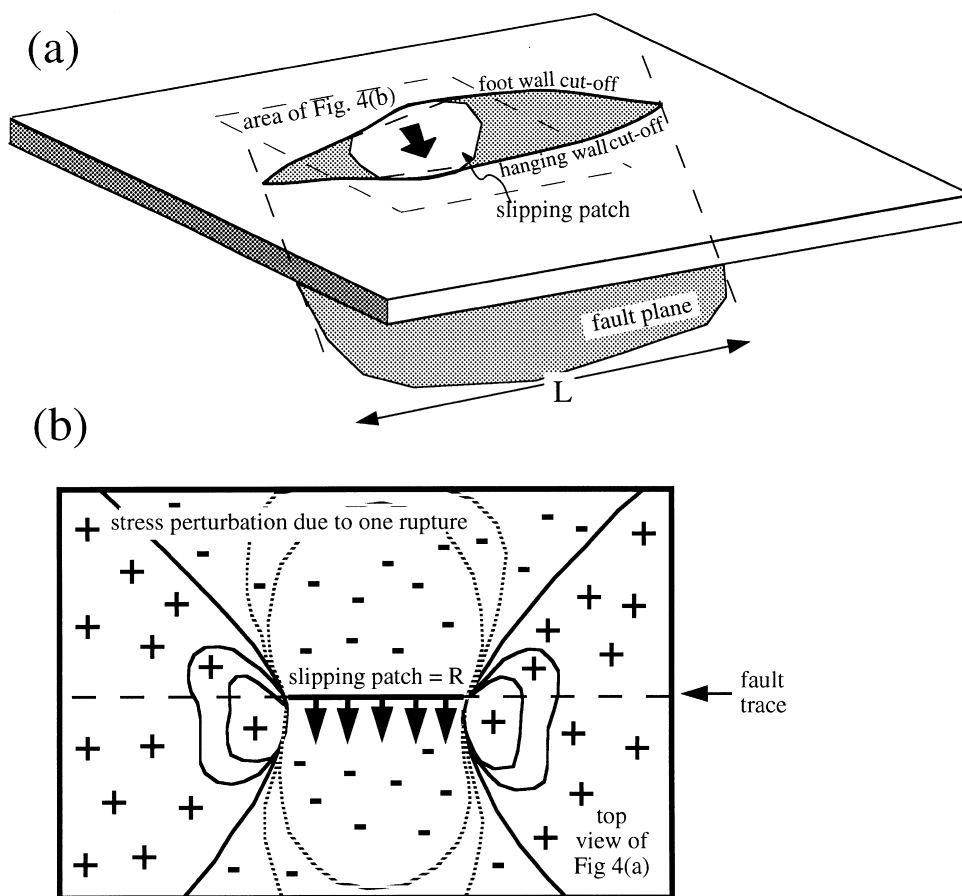
(a)

(b)

Fig. 4. (a) Sketch showing a dipping normal fault which ruptures over a small portion of its length while adjacent parts of the fault remain healed. (b) Change in stress in the region around the slipping patch: + signs indicate regions of increased likelihood for failure on planes parallel or co-planar to the plane of the rupture; − signs indicate reduced likelihood for failure (modified from Hodgkinson *et al.*, 1996). See text for discussion.

rupture zone. The stress variation shown in Fig. 4(b) is qualitatively very similar to a vertical dip-slip fault (i.e. a pure Mode III crack) and thus we make that approximation in the modelling presented below. In this paper we do not refer explicitly to strike-slip faults (or Mode II fault tips). In that case the stress perturbation is asymmetric with respect to the rupture zone (King *et al.*, 1994), but the basic mechanism of healing and reloading should still be applicable.

NUMERICAL MODELLING

The process of localised slip, healing (i.e. strength recovery) and stress reloading is demonstrated by a model for fault growth presented by Cowie *et al.* (1993), Sornette *et al.* (1994) and Cowie *et al.* (1995). They show the results of a two-dimensional lattice model for anti-plane shear of a thin plate, using a scalar calculation of the stress field. Each element of the lattice is assigned a random strength value and failure occurs locally when this strength is exceeded. Imposed tectonic loading at a constant strain rate causes elements to reach failure, and an abrupt stress drop is

applied to an element when it fails. The resulting stress perturbation is distributed on neighbouring elements such that forces induced by rupture are balanced over the surrounding area. Because in this model an element recovers its strength instantaneously after rupture, the area over which the force balance is calculated includes previously healed elements as well as those that have never ruptured. Thus the stress level on all elements in the lattice at any point in time is due to a combination of (a) the tectonic loading and (b) re-loading caused by other ruptures.

For the case of anti-plane shear, modelled by Cowie *et al.* (1993), regions of stress increase lie along strike from a rupture (Mode III shear; Pollard and Segall, 1987). Because of this symmetry property of the stress perturbation around each ruptured element and the inclusion of instantaneous healing, a positive feedback develops between nearby ruptures that are aligned approximately along-strike. The deformation localises and displacement accumulates because of this positive stress feedback effect. The resulting fault displacement profiles are controlled by a balance between accumulation of displacement on previously ruptured elements, new ruptures forming at the tips, and linkage

with other nearby faults. Figure 5(a) shows an example of a typical fault displacement profile at one stage of the model evolution, and a real data set for comparison taken from Dawers and Anders (1995) (Fig. 5b). The tip gradients of the model fault are finite, and no tapering of the profile is seen which is very similar to the natural example.

The Cowie *et al.* (1993) model implicitly obeys the theory of PYFM because the stress level is everywhere limited by the finite strength levels in the lattice. The size of the frictional breakdown zone, *s*, is not explicitly defined but its length is necessarily less than the lattice element dimensions which defines the size of each rupture *R*. Thus *s* is not visible at the scale of Fig. 5(a). The size *R* is assumed here to be 300 m, as this model is a thin plate approximation and we wish to compare it to the faults in the Bishop Tuff which is approximately 300 m thick (Dawers and Anders, 1995). The magnitude of slip each time an element ruptures is calculated by assuming that the maximum supportable elastic strain before failure is of the order of 10^{-2}. For a 100% stress drop at rupture, this elastic strain is converted into a permanent strain which is an increment of accumulated displacement on a fault. The displacement profiles observed in this model are influenced by a combination of fault interaction, growth by linkage, and heterogeneous material properties. Moreover the fault traces are multi-stranded and irregular. These are the reasons for comparing, in Fig. 5, the model fault to a linked fault array rather than an isolated single fault. In order to study how the healing and stress feedback mechanism operates at the scale of an isolated fault tip a simplified model is required.

In this paper we present a two-dimensional model for a single planar fault. The purpose of this simplified model is to demonstrate that self-similar fault growth is achieved, and in fact is controlled by, the stress feedback mechanism. The aim is also to show: (a) how a finite tip displacement gradient is built up and sustained, (b) how tip profiles may be characterised in field data collection, and (c) how rock properties may influence such measurements. In other respects, qualitative differences between profiles produced by the simplified model and the model of Cowie *et al.* (1993) can be attributed to the planar fault approximation.

Planar fault model

Following the antiplane modelling approach presented by Cowie *et al.* (1993), we consider the stress perturbations due to ruptures on an isolated planar vertical dip-slip fault and study the resulting bilateral propagation. The major assumption made in the construction of this simple model is that these rupture-induced stress perturbations dominate over the influence of tectonic loading. Thus, propagation of the fault tip is due entirely to the stress concentration resulting from displacement accumulation on the fault, rather than being caused by tectonic stresses imposed remotely. Consequently, we are able to examine the propagation of an isolated tip without the complicating effect of neighbouring faults beginning to nucleate and then interact. The model is produced by assigning to each element along a linear array a strength value which is drawn randomly from a flat probability distribution between two limits: σ_{min}, the minimum strength, and σ_{max}, the maximum strength. This produces a uniformly random heterogeneity about a constant average strength. The stress level required to break the weakest element defines the regional stress $(=\sigma_{min})$ which is applied to all the elements (Fig. 6). An instantaneous stress drop occurs on the broken ele-
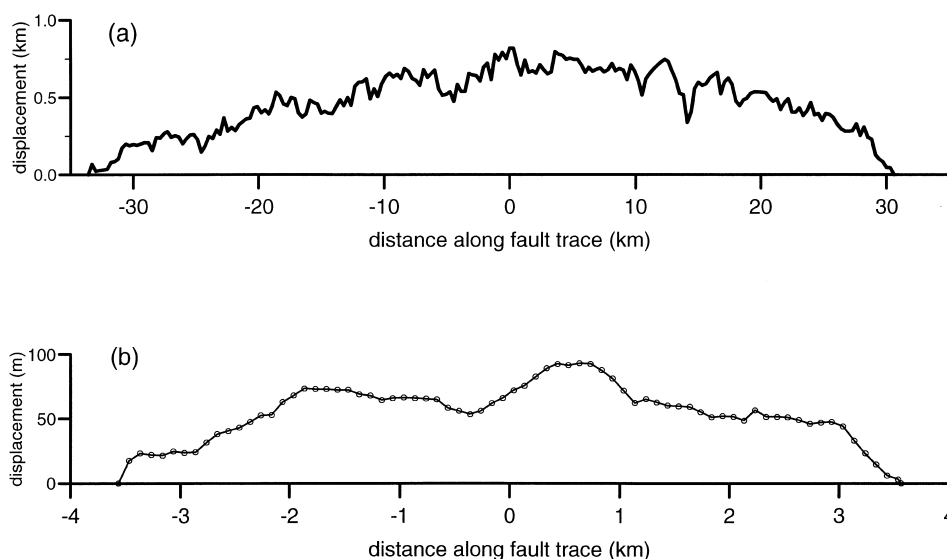

Fig. 5. (a) Displacement profile along a fault zone generated using the lattice rupture model of Cowie *et al.* (1993), compared with (b) a displacement profile measured by Dawers and Anders (1995) along a linked normal fault in Owen's Valley, California, U.S.A. See text for discussion.
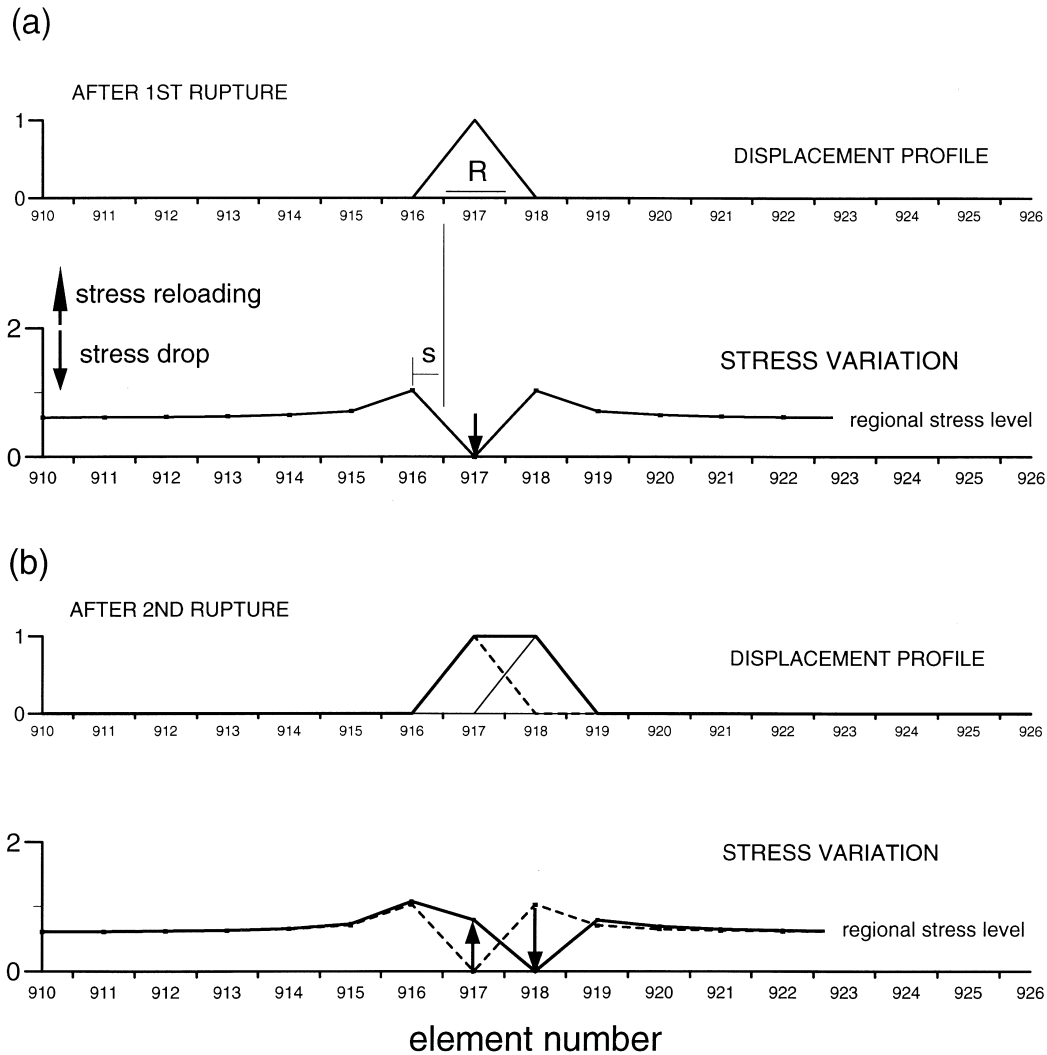
(a)

(b)

Fig. 6. Displacement distributions and stress variations for the planar fault model after (a) the first and (b) the second rupture events. Arrows indicate stress drop where rupture occurs and in (b) stress reloading of a previously ruptured element. See text for details.

ment and an increase in stress is imposed on the neighbours (Fig. 6). New ruptures are triggered in this way and not by any other loading mechanism, such as tectonic loading. Rupture is modelled as a 100% stress drop and inertial effects are not included. Thus the stress drop is assumed to be gradual compared to seismic rupture nucleation, but still instantaneous compared to the duration of fault development.

The increase in stress on the neighbours immediately adjacent to each rupture is limited by the strength of the weaker of the two neighbours, σ_i (Fig. 6). This is the constraint imposed by the theory of PYFM. A frictional breakdown zone, of length s, is thus implicitly included at the tips of each rupture, R, so that $s < R/2$ and in this model R is a constant. We consider only the stress changes in the plane of the fault. The stress perturbation to either side of the rupture is modelled here by a decrease in stress with distance according to $(\sigma_i - \sigma_{min})(R/(2r + R))^2$ where R is the size of each element and r is the distance away from each end of the

rupture (Fig. 6). This expression describes the decay in shear stress beyond the tips of a Mode III crack with uniform loading and is thus only valid at distances, $r > R/2$. At distances, $r \sim R/2$ the tip stress singularity is strongly suppressed by the presence of the end zone, s, compared to the simple elastic crack model (Willemse and Pollard, 1998). For the nearest neighbour elements this effect is taken into consideration by setting the peak stress equal to σ_i. For elements at further distances the approximation is valid, but only to first order (cf. Pollard and Segall, 1987; Willemse and Pollard, 1998). The justification for ignoring changes in normal stress induced by rupture is made in the Conceptual Framework section above.

Only one element is allowed to break at a time and it is always the most critically stressed element, i.e. the element which has the greatest difference between its breaking stress and the applied stress. A ruptured element heals instantaneously so that at any point in time only one element suffers a drop in stress and any

previous breaks are gradually reloaded towards failure once more by adding together the stress perturbations from all previous breaks. Figure 6 illustrates how the model works for the first two rupture events. The first break occurs at $x = 917$ and it triggers the next rupture to occur at $x = 918$. Because the element at $x = 917$ has healed instantaneously, it becomes reloaded by the subsequent event, as indicated by the arrows. The simple slip profile associated with each rupture is also shown in Fig. 6. We ignore the details of the profile that would result if the zone s is explicitly modelled for each slip event (see Burgmann *et al.* (1994) for the full mathematical solution for the slip profile along a shear crack with a frictional breakdown zone at its ends).

Figure 7 shows an example of the model results for a fault at one point in time in its evolution when $L = 870$ m and $D = 11$ m. Each element is assumed to be 1 m long and the increment of displacement due to each rupture is obtained by assuming that the maximum supportable elastic strain before failure is of the order of 10^{-2}, i.e. 1 cm. The displacement profile in the vicinity of the left hand fault tip is shown in Fig. 7(a). Figure 7(b) shows the distribution of stress compared to the strength of the material through which the fault is propagating. The strength varies randomly about an average value of 1.0 with $\sigma_{max} = 1.4$ and $\sigma_{min} = 0.6$ in this case. A new random strength is assigned to an element each time it ruptures, but no systematic weakening of ruptured elements is taken into consideration. Weakening is not a necessary ingredient for demonstrating the process of interest here. The displacement profile has an approximately constant gradient maintained as far as the tip itself (Fig. 7a). Note that s would not be discernible at the scale of this diagram as it is $< R/2$, i.e. < 50 cm. For comparison, an elliptical displacement profile for a fault of the same D and L is plotted.

Along the length of the fault the stress fluctuates strongly, reflecting the continual process of rupturing and reloading after each rupture event (Fig. 7b). The regional stress level is also indicated and is approximately the same as the average level on the fault. At the tip of the fault the stress is approximately equal to the strength at that point (Fig. 7b). Beyond the tip the stress decays rapidly to the background level. Although some elements beyond the tip have a stress level that exceeds their strength, rupture only occurs when this 'stress excess' is larger than for any other element, as explained above. In Fig. 7 only one element beyond the tip has reached this level and it has been assigned a new random strength when it ruptured. The rapid decay of the stress beyond the tip is a significant feature of this model. In Fig. 7(b) the distance at which the stress has decayed to 10% above the regional level is 112 m which is approximately 13% of the fault length, L. Figure 7(c) shows a plot of the decay distance (the distance from the tip where the
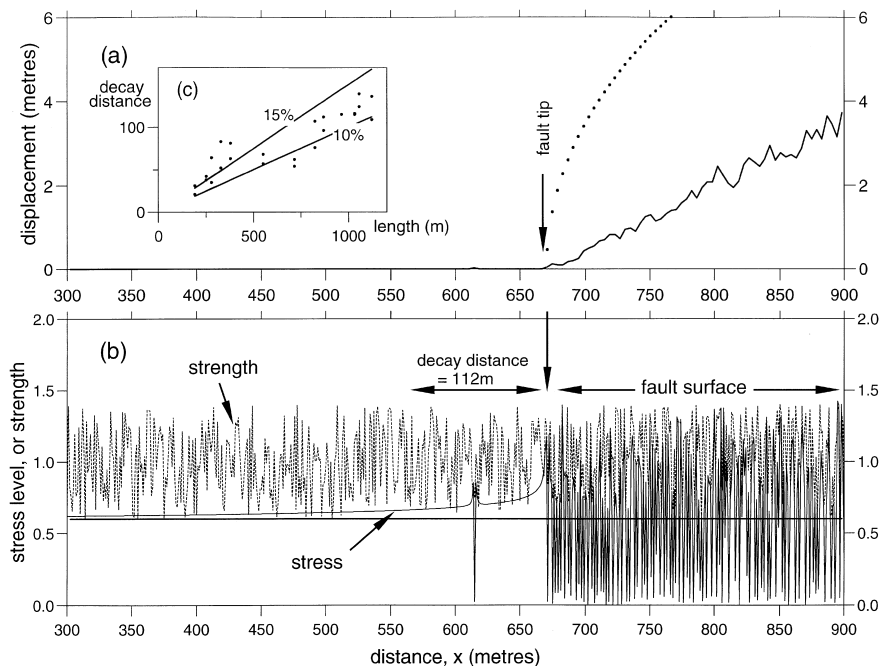

Fig. 7. Displacement profile and stress distribution near the left hand tip of a fault generated using the planar model. The fault extends from $x = 670$ m to $x = 1540$ m, giving a total length $L = 870$ m, and the size of one element is 1 m. (a) Displacement profile on the fault showing an approximately linear decrease towards the tip. Dots indicate an elliptical profile for a fault with the same D and L. (b) Stress (solid line) compared to the strength of the material (dashed line). The strength properties vary randomly and no mechanical weakening of the fault is included. The stress decays rapidly beyond the fault tip to 10% above the regional stress at ~112 m from the tip—the 'decay distance'. (c) Correlation between L and decay distance at different stages of growth of the same fault. Lines indicate approximate range of values, i.e. decay distance is consistently about 10–15% of L.
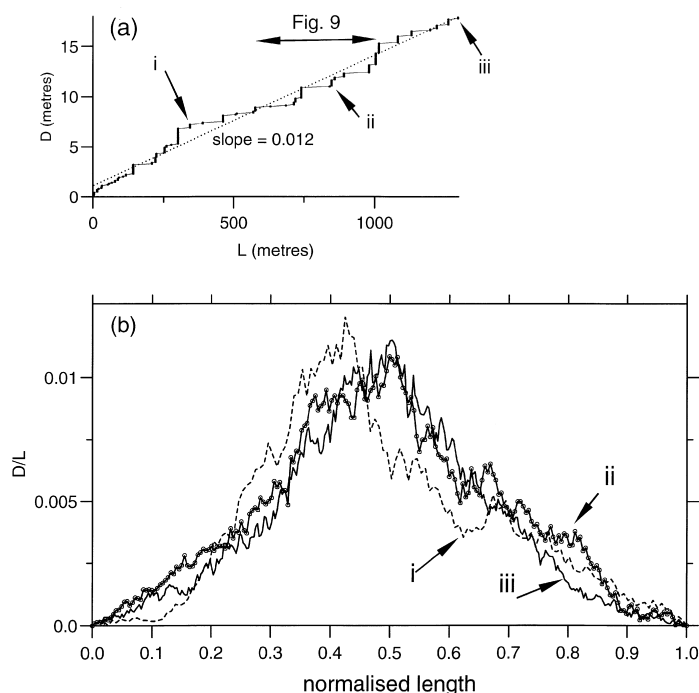
Fig. 8. Self-similar growth using the planar fault model. (a) D as a function of L during the progressive growth of an individual fault. Overall the growth is self-similar with average $D/L = 0.012$. (b) Normalised displacement profiles calculated at three successive points in the fault growth history [indicated as i, ii, iii in (a)].

stress has fallen to 10% above regional) against L for this simulation. The decay distance scales with L with a range of values between $0.1L$ and $0.15L$ although there is some scatter. The implication of this result for interaction between faults is discussed in the next section.

Figure 8 demonstrates the self-similar growth through time of the fault shown in Fig. 7. Figure 8(a) shows D as a function of L and illustrates a step-like growth behaviour, i.e. periods when displacement accumulates with insignificant fault lengthening followed by periods in which lengthening predominates. This inherently discrete growth behaviour is a consequence

of the heterogeneous strength properties. The average rock strength controls the overall scaling and the average D/L ratio. Figure 8(b) is a normalised plot of three fault displacement profiles for the same fault at different points during the evolution shown in Fig. 8(a). The profiles are approximately triangular in shape with the maximum near the centre close to, but not always coincident with, the point of nucleation. The individual profiles are not identical and often show asymmetry and the profile shape continues to change as the fault grows. The apparent shift in the position of the maximum displacement seen in Fig. 8(b) is a consequence of normalising profiles which are asym-
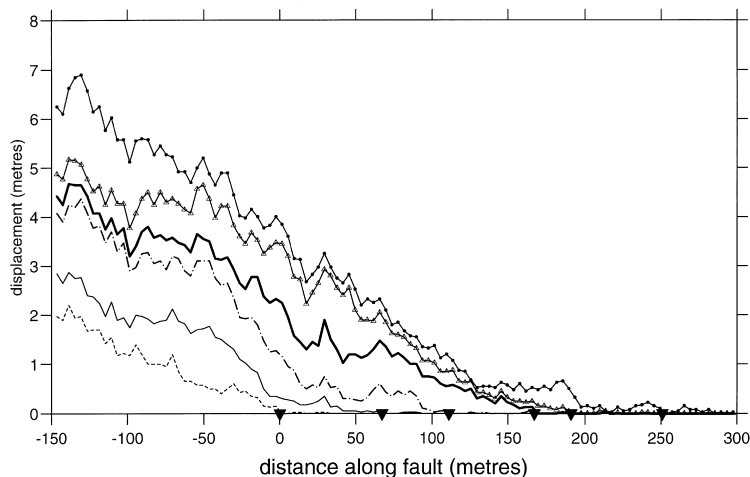

Fig. 9. Time evolution of the displacement profile behind the right hand tip for the fault shown in Fig. 7. (a) Six successive profiles in the growth history (indicated in Fig. 8a). The black triangles indicate the fault tip position at each stage, defined as the point where the displacement first falls to zero away from the centre of the fault.

metric. The progressive growth of the fault is clearly irregular in detail but overall the scaling is self-similar. This is consistent with the linear relationship between the decay distance and L shown in Fig. 7(c).

Figure 9 shows the actual tip propagation of the fault at six different stages in its evolution (see Fig. 8a). The evolution of the displacement profile in the vicinity of the tip is controlled by three main processes: (1) the formation of a few isolated ruptures just in front of the tip, (2) the linking of these to the main fault, and (3) building up of displacement behind the fault tip. The competition between these processes produces significant variability in the profiles during propagation but overall it moves forward maintaining a wedge-like profile with displacement accumulation behind the fault tip being balanced by fault propagation. This balance is the manifestation of the stress feedback mechanism operating to achieve and maintain a steady-state profile for the actively growing fault.
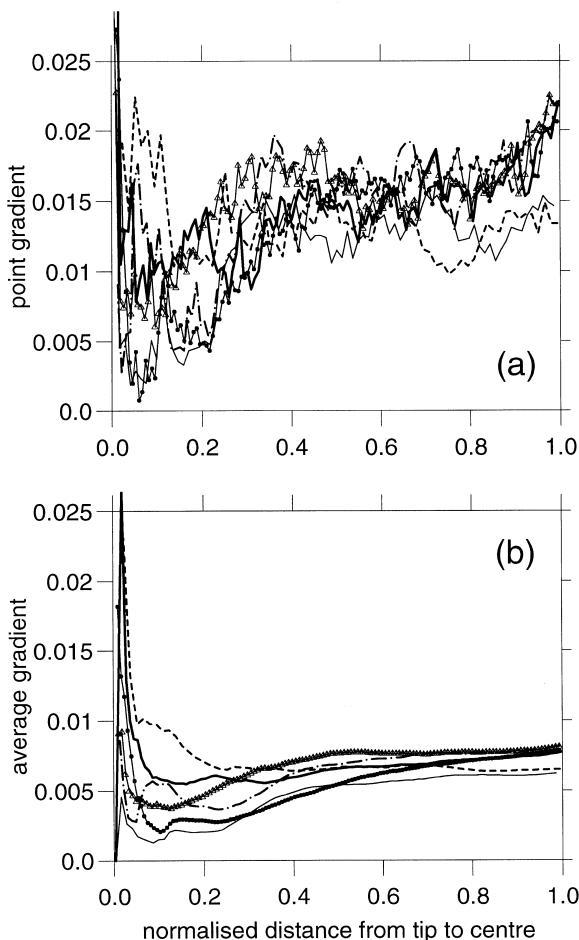

Fig. 10. (a) Point and (b) average displacement gradients calculated as a function of normalised distance from the tip (0.0) to the centre of the fault (1.0) for the profiles shown in Fig. 9. Symbols are the same as in Fig. 9. See text for discussion.

Figure 10 shows a quantitative analysis of the tip gradients shown in Fig. 9. The displacement gradients are calculated as a function of distance from the tip to the centre of the fault for each of the six profiles. Two methods are used: the point gradient (Fig. 10a) and the average gradient (Fig. 10b). The first method uses directly the displacement at each point divided by the distance behind the tip. The average gradient is obtained by averaging the displacement up to a given distance behind the tip and dividing by this distance. The point gradient fluctuates strongly, showing an order of magnitude variation, and does not clearly distinguish between the profiles (Fig. 10a). In contrast the average gradient varies smoothly and, beyond some distance behind the tip, the gradients are approximately the same and constant. Significant differences between consecutive profiles are clear between 10% and 20% of the distance to the mid-point of the fault (Fig. 10b). This range is remarkably similar for all the faults, suggesting that the length of the region over which the tip gradient becomes established depends on the dimensions of the fault, rather than the scale of the heterogeneity. The simplicity of the model means that the length of this region (10–20%) cannot be directly related to real faults. The important point is that the details of the tip profile are very sensitive to local heterogeneity, particularly if this heterogeneity is strong: e.g. a heavily fractured or layered rock mass.

DISCUSSION

Frictional slip mechanism and fault strength recovery

One of the key ingredients in the model results presented above is the assumption that individual ruptures only occur over a small portion of a fault. This is probably the most realistic scenario in sedimentary rocks which generally have a lower stiffness and lower peak strength compared to crystalline materials, and thus store little elastic strain energy before failing. Faults which slip by this mechanism may produce micro-seismicity rather than moving in major earthquakes. Materials that exhibit slip-weakening but not velocity-weakening, e.g. serpentine and clay, would also be consistent with slip only occurring over very small patches, probably aseismically. However, even major seismogenic faults exhibit a range of event size; they do not only move in events that rupture their entire length. Thus, even though the present model does not address dynamic rupture explicitly we believe that healing and positive stress feedback must still apply and affect the accumulation of displacement on faults of all types.

Another assumption of the model is that ruptured elements recover their strength instantaneously and are able to support stress increases resulting from subsequent ruptures. Heimpel (1997) shows, using a nu-

merical model, that frictional shear strength of a rough fault gradually increases after earthquake rupture due to interlocking of asperities. Cataclastic deformation inherently leads to an evolving population of asperities as the fault moves. Although complete strength recovery is not found to be instantaneous in this model, the most significant increase occurs shortly after rupture has stopped. Recent experimental results (Marone, 1998) show that immediate post-seismic healing may be retarded for a period of several hundred days due to compaction effects, but on longer time scales the rate of increase is of the order of 3–6 MPa per decade. Chemically assisted healing probably plays an important role in natural faults due to precipitation of minerals, such as quartz and calcite, and annealing of micro-cracks. Annealing under geological conditions is thought to occur very rapidly, i.e. within a few months (e.g. Smith and Evans, 1984; Brantley *et al.*, 1990). All of these processes are instantaneous compared to the life-span of a fault and the recurrence time of slip events on most faults.

Slip patch dimensions

In this model, the slip patch dimension, R, is assumed to be a constant and approximately linear tip profiles are found to be well developed when $R \ll L$. Using a constant value of R is merely a mathematical convenience and, as mentioned above, there is plenty of evidence to suggest that seismogenic faults often rupture in events of different sizes. Thus, in nature R is variable and $R \ll L$ is not always the case. It is relevant therefore to note that a similar profile shape was obtained by Mavko (1982) using an analytical method for calculating the slip distribution along a crack with a heterogeneous stress drop. He described the stress fluctuations using Chebyshev polynomials of different order; higher order functions giving shorter wavelength fluctuations. Although he considered a static crack with a static stress distribution, the correspondence with the results of the present model suggest that $R \ll L$ is not a necessary condition for producing displacement profiles that show an approximately linear decrease towards the tip. For example, stress fluctuations with a wavelength of 10–20% L, particularly close to the tip, are sufficient to eliminate any tapering of the profile shape. The importance of the present work is that a mechanism is provided to explain why such stress fluctuations arise, one that is common to faults in general and not dependent on specific details of rheological layering or interaction with other faults.

Process zone scaling

According to C&S92 the size of the frictional breakdown zone, s, scales with R. Therefore we would predict that, if R is constant, any micro-cracked process zone that is preserved around the fault will have an approximately constant width, P, along the fault trace, although the intensity of micro-cracking will be a maximum where the displacement is largest because of repeated slip in this area. If we now consider a more general case in which R is not a constant but still $R < L$, then we would expect to see variability in the width of P associated with each slip event but again it may not be clearly related to the overall displacement profile on the fault. For example, the width P may increase overall around larger faults, as they have probably suffered larger slip events, but is unlikely to show systematic widening along the length of the fault as predicted by Scholz *et al.* (1993) and Anders and Wiltschko (1994). The results of Vermilye (1996) could provide support for this argument: she found that the scaling of process zone width with length is approximated by $P/L \sim 0.01$, which is an order of magnitude smaller than that estimated by C&S92. If we assume, for example, that for the largest events on those faults studied by Vermilye, $R \sim 0.1L$ and $s \sim 0.1R$ (from C&S92), then these results are internally consistent. Moreover, Vermilye (1996) found that micro-fracture orientations in the process zone could not be explained by sequential slip events each affecting the whole fault. Instead she observed individual segments along which several slip events could be identified, sometimes showing opposite propagation directions.

Influence of rock strength and rock heterogeneity

In the results presented a fault maintains, on average, a self-similar tip displacement profile as it propagates. This is achieved by a combination of tip propagation and accumulation of displacement behind the tip. In detail, growth occurs in an irregular fashion due to the presence of heterogeneities in the material properties. The heterogeneities consist of a uniformly random fluctuation in shear strength about a mean value. For real faults, variability in tip gradients is expected even without invoking major contrasts in rock type or rheological behaviour, as has been proposed by Burgmann *et al.* (1994). In other words, heterogeneities within the same overall lithology may produce significant variations. The magnitude of this effect is probably less important than that due to fault interaction, see for example Peacock and Sanderson (1991) and Willemse *et al.* (1996), unless the lithology is highly jointed (e.g. Cartwright and Mansfield, 1998). Dawers *et al.* (1993) found that, for isolated faults in a relatively simple tectonic setting, some asymmetry and variability in tip gradient measurements is common, probably due to the presence of joint sets in that area. Our results indicate that the average tip gradient provides a robust measurement for characterising profiles but depends on having sufficient displacement data rather than one single measurement at a point (cf. Cartwright and Mansfield, 1998).

The heterogeneity in strength properties influences the ratio D/L. Although on average D and L are correlated, in detail the growth of the fault occurs either by increments of displacement, with no lengthening, or by rapidly increasing the length with little change in displacement. This kind of growth behaviour has been attributed to the role of fault linkage (Cartwright *et al.*, 1995), but here it is a consequence of the variable rock strength. A least-squares fit through a plot of D vs L is a measure of the average rock strength in this model. The mathematical expressions relating D/L to *in situ* rock properties given by C&S92 and Burgmann *et al.* (1994) are no longer directly applicable; they are appropriate to the individual ruptures but not the whole fault.

Fault interaction

The stress field beyond the tip of the model faults decays rapidly with distance. Within a distance of 10–15% of L beyond the tip the stress has decayed to 10% above the regional stress level. This is a consequence of the fact that the range of the stress perturbation due to an individual slip event is controlled by the size of R, and $R < L$. Ruptures occurring towards the centre of the fault have little direct influence on the stress level at the tip of the fault when $R \ll L$. For example, Fig. 6 shows that the perturbation due to an individual rupture has decayed substantially within a distance of approximately $3R$. In this model, the stress decay beyond the fault tip is thus primarily controlled by the displacement distribution immediately behind the tip. The implication of this result is that the maximum distance over which two faults could be said to interact strongly will be rather limited if faulting is occurring by the proposed mechanism. This is a significant result, as faults separated by a distance which is relatively short compared to their length may not show evidence of interaction, i.e. asymmetric displacement profiles and steep tip gradients (Peacock and Sanderson, 1991). Previous calculations of interaction distances, based on static elastic crack models with uniform loading, predict significantly greater interaction distances, i.e. $L/2$ (Burgmann *et al.*, 1994), unless a high-aspect ratio three-dimensionality of the fault plane is included (Willemse, 1997). Note that the interaction referred to here concerns near-field effects which are strong enough to modify fault displacement profiles. The long range interaction described by Cowie *et al.* (1993) is still present in the model but is a far-field effect which is of very low amplitude.

CONCLUSIONS

A model has been presented which may explain the observation that faults commonly exhibit finite and approximately linear tip displacement gradients. The fundamental assumption which we make is that the plane of a fault, as well as the surrounding rock volume, support the stress perturbations associated with a slip event. This reduces the stress concentration around the fault tip and also leads to spontaneous self-reloading of the fault as stress is transferred from the portion that is slipping to portions that are healed. We call this the stress feedback effect. The peak stress due to each slip event is limited by the local material strength. We modify the theory of post-yield fracture mechanics, applied to faults by C&S92, by scaling the process zone, or frictional breakdown zone, s, with the size of the instantaneous rupture dimensions, R, rather than the length of the fault, L. Therefore, if $R \ll L$, s becomes very small. The other extreme is when $R \sim L$ for each rupture in which case s does scale with L. In the former case a small patch of the fault is slipping at any point in time and the rest of the fault is healed. The model depends on the rate of healing, i.e. strength recovery, being short compared to the time interval between subsequent ruptures.

We have shown, using a simple rupture model for a single planar dip-slip fault, that for $R \ll L$ the tip displacement profiles show an approximately linear decrease towards the tip comparable to natural examples. The finite gradient is achieved by a balance between displacement accumulation behind the tip and forward propagation of the tip. The balance is controlled by the stress feedback between slipping and healed portions of an actively growing fault. We suggest that this mechanism is common to all faults, and is particularly relevant to faults forming in sedimentary rocks which are less rigid and have lower shear strengths compared to crystalline rocks. The proposed mechanism certainly seems applicable to faults forming in analogue experiments which show displacement profiles very similar to natural examples. The bell-shaped displacement profiles predicted by the C&S92 model will only form if $R = L$. Identifying a bell-shaped profile from field observations might therefore indicate a fault that has predominantly moved in major seismic events that rupture the entire fault, although other factors such as changing bulk rheology may also play a role. If R is variable throughout a fault's history, such that $R \leq L$, then the tapered shape of the displacement profile is less well developed. In this case the process zone wake may record the extent and direction of propagation of individual events, especially the largest.

In the model the stress level at the tip of the growing fault is maintained close to the local rock strength. An overall linear correlation between maximum displacement and fault length is observed but the growth history of an individual fault does not simply follow a single growth trajectory. Instead there are periods of growth where displacement accumulates and the length changes little, followed by significant increase in length with only a small increment of displacement. The

resulting 'stepped' growth curve results from heterogeneity in rock strength used in the model and introduces scatter in the displacement–length correlation plot. This effect is small compared to other processes like fault tip interaction, linkage and changes in overall rock rheology, but will lead to intrinsic variability and asymmetric profile shapes in displacement data derived from apparently simple systems of faults. The average D/L ratio reflects the average shear strength of the rock in which the fault is growing.

A discriminating measurement of tip profile shape is obtained by calculating the average gradient as a function of distance behind the tip. In the presence of strong local variability in rock strength, e.g. pervasive jointing, profile data that extend some distance behind the tip (>0.1–$0.2L$) are required to fully characterise the profiles. Thus to resolve subtle effects such as incipient interaction with nearby structures, detailed measurements over considerable distances are probably necessary. According to this model, the stress decays to 10% above the regional stress level at a distance 0.1–$0.15L$ from the fault tip. The decay distance scales linearly with fault length, as we would expect for self-similar growth, but the stress concentration is much more limited than for simple two-dimensional elastic crack models for which this same decay occurs over a distance $L/2$. Thus strong interaction between neighbouring structures may only occur if they are separated by a distance that is short compared to their length, regardless of their three-dimensional geometry.

Finally, the mechanism of stress feedback described here may have wider implications for the long time-scale evolution of segmented fault zones. We have only considered an extreme case of a single fault in which slip and rehealing of small patches lead to spontaneous reloading of adjacent parts of the same fault plane. This basic idea may also apply to the co-planar segments of a fault zone where only one or two segments rupture in individual earthquakes and the rest are healed. The mechanism of earthquake triggering, i.e. one event inducing others on nearby faults (e.g. Stein et al., 1992; Hodgkinson et al., 1996), is the short-time-scale manifestation of this effect. Cowie (1998) looks at the integrated effect over geological time, showing how stress feedback between active faults results in systematic variations in rates of growth along segmented fault arrays.

REFERENCES

Anders, M. H. and Wiltschko, D. V. (1994) Microfracturing, paleostress and the growth of faults. *Journal of Structural Geology* **16**, 795–816.

Antonellini, M. A., Aydin, A. and Pollard, D. D. (1994) Microstructure of deformation bands in porous sandstones at Arches National Park, Utah. *Journal of Structural Geology* **16**, 941–959.

Aydin, A. (1978) Small faults formed as deformation bands in sandstone. *Pure and Applied Geophysics* **116**, 913–929.

Aydin, A. and Johnson, A. (1978) Development of faults as zones of deformation bands and as slip surfaces in sandstones. *Pure and Applied Geophysics* **116**, 931–942.

Aydin, A. and Johnson, A. (1983) Analysis of faulting in porous sandstones. *Journal of Structural Geology* **5**, 19–31.

Barr, T. D. and Houseman, G. A. (1996) Deformation fields around a fault embedded in a non-linear ductile medium. *Geophysical Journal International* **125**, 473–490.

Brantley, S. L., Evans, B., Hickman, S. H. and Crerar, D. A. (1990) Healing of microcracks in quartz: implications for fluid flow. *Geology* **18**, 136–139.

Burgmann, R., Pollard, D. D. and Martel, S. J. (1994) Slip distributions on faults: effects of stress gradients, inelastic deformation, heterogeneous host-rock stiffness, and fault interaction. *Journal of Structural Geology* **16**, 1675–1690.

Cartwright, J., Mansfield, C. and Trudgill, B. (1995) The growth of faults by segment linkage: Evidence from the Canyonlands grabens of S. E. Utah. *Journal of Structural Geology* **17**, 1319–1326.

Cartwright, J. A. and Mansfield, C. S. (1998) Lateral tip geometry and displacement gradients on normal faults in the Canyonlands National Park, Utah. *Journal of Structural Geology* **20**, 3–19.

Cowie, P. A. (1998) A healing–reloading feedback control on the growth rate of seismogenic faults. *Journal of Structural Geology.* **20**, 1075–1087.

Cowie, P. A. and Scholz, C. H. (1992) Physical explanation for displacement–length relationship for faults using a post-yield fracture mechanics model. *Journal of Structural Geology* **14**, 1133–1148.

Cowie, P. A., Vanneste, C. and Sornette, D. (1993) Statistical physics model for the spatio-temporal evolution of faults. *Journal of Geophysical Research* **98**, 21809–21822.

Cowie, P. A., Sornette, D. and Vanneste, C. (1995) Multifractal scaling properties of a growing fault population. *Geophysical Journal International* **122**, 457–469.

Dawers, N. H. and Anders, M. H. (1995) Displacement-length scaling and fault linkage. *Journal of Structural Geology.* **17**, 607–614.

Dawers, N. H., Anders, A. and Scholz, C. H. (1993) Growth of normal faults: Displacement-length scaling. *Geology* **21**, 1107–1110.

Edwards, H. E., Becker, A. D. and Howell, J. A. (1993) Compartmentalisation of an aeolian sandstones by structural heterogeneities: Permo-Triassic Hopeman Sandstone, Moray Firth, Scotland. In *Characterisation of Fluvial and Aeolian Reservoirs.* eds C. P. North and D. J. Prosser. Geological Society of London Special Publications **73**, pp. 339–365.

Gillespie, P. A., Walsh, J. J. and Watterson, J. (1992) Limitations of displacement and dimension data for single faults and the consequences for data analysis and interpretation. *Journal of Structural Geology* **14**, 1157–1172.

Gross, M. R., Gutierrez-Alonso, G., Bai, T., Wacker, M. A., Collinsworth, K. B. and Behl, R. J. (1997) Influence of mechanical stratigraphy and kinematics on fault scaling relationships. *Journal of Structural Geology* **19**, 171–183.

Heimpel, M. (1997) Critical behaviour and the evolution of fault strength during earthquake cycles. *Nature* **388**, 865–868.

Hodgkinson, K. M., Stein, R. S. and King, G. C. P. (1996) The 1954 Rainbow Mountain–Fairview Peak–Dixie Valley earthquakes: A triggered normal faulting sequence. *Journal of Geophysical Research* **101**, 25459–25471.

King, G. C. P., Stein, R. S. and Lin, J. (1994) Static stress changes and the triggering of earthquakes. *Bulletin of the Seismological Society of America* **84**, 935–953.

Krantz, R. W. (1988) Multiple fault sets and three-dimensional strain: theory and application. *Journal of Structural Geology* **10**, 225–237.

Mansfield, C. S. (1996) Fault growth by segment linkage. Ph.D. thesis, Imperial College, London.

Marone, C. (1998) The effect of loading rate on static friction and the rate of fault healing during the earthquake cycle. *Nature* **391,** 69–72.

Martel, S. J. and Pollard, D. D. (1989) Mechanics of slip and fracture along small faults and simple strike-slip fault zones in granitic rock. *Journal of Geophysical Research* **94,** 9417–9428.

Mavko, G. M. (1982) Easy computation of static stress drop, slip and moment on two-dimensional heterogeneous faults. *Bulletin of the Seismological Society of America* **72,** 1499–1508.

Muraoka, H. and Kamata, H. (1983) Displacement distribution along minor fault traces. *Journal of Structural Geology* **5,** 483–495.

Nicol, A., Watterson, J., Walsh, J. J. and Childs, C. (1996) The shapes, major axis orientations and displacement patterns of fault surfaces. *Journal of Structural Geology* **18,** 235–248.

Peacock, D. C. P. and Sanderson, D. J. (1991) Displacements, segment linkage and relay ramps in normal fault zones. *Journal of Structural Geology* **13,** 721–733.

Peacock, D. C. P. and Sanderson, D. J. (1996) Effects of propagation rate on displacement variations along faults. *Journal of Structural Geology* **18,** 311–320.

Pickering, G., Peacock, D. C. P., Sanderson, D. J. and Bull, J. M. (1997) Modelling tip zones to predict the throw and length characteristics of faults. *Bulletin of the American Association of Petroleum Geologists* **18,** 82–99.

Pollard, D. D. and Segall, P. (1987) Theoretical displacements and stresses near fractures in rock: with applications to faults, joints, veins, dikes, and solution surfaces. In *Fracture Mechanics of Rock*, ed. B. K. Atkinson, pp. 277–349. Academic Press, New York.

Schlische, R. W., Young, S. S., Ackermann, R. V. and Gupta, A. (1996) Geometry and scaling relationships of a population of very small rift-related normal faults. *Geology* **24,** 683–686.

Scholz, C. H., Dawers, N. H., Yu, J.-Z., Anders, M. H. and Cowie, P. A. (1993) Fault growth and fault scaling laws: preliminary results. *Journal of Geophysical Research* **98,** 21951–21962.

Smith, D. L. and Evans, B. (1984) Diffusional crack healing in quartz. *Journal of Geophysical Research* **89,** 4125–4135.

Sornette, D., Miltenberger, P. and Vanneste, C. (1994) Statistical physics of fault patterns self-organised by repeated earthquakes. *Pure and Applied Geophysics* **142,** 491–527.

Stein, R. S., King, G. C. P. and Lin, J. (1992) Change in failure stress in the southern San Andreas Fault System caused by the 1992 magnitude 7.4 Landers Earthquake. *Science* **258,** 1328–1332.

Underhill, J. R. and Woodcock, N. H. (1987) Faulting mechanisms in high porosity sandstones, New Red Sandstone, Arran, Scotland. In *Deformation of Sediments and Sedimentary Rocks*, eds M. E. Jones and R. M. F. Preston, Geological Society of London Special Publications, **29,** pp. 91–105.

Vermilye, J. (1996) The growth of natural fracture systems: A fracture mechanics approach. Ph.D thesis. Columbia University, New York.

Walsh, J. J. and Watterson, J. (1987) Distribution of cumulative displacement and seismic slip on a single normal fault surface. *Journal of Structural Geology* **9,** 1039–1046.

Walsh, J. J. and Watterson, J. (1988) Analysis of the relationship between displacements and dimensions of faults. *Journal of Structural Geology* **10,** 239–247.

Willemse, E. J. M., Pollard, D. D. and Aydin, A. (1996) Three-dimensional analysis of slip distributions on normal fault arrays with consequences for fault scaling. *Journal of Structural Geology* **18,** 295–310.

Willemse, E. J. M. (1997) Segmented normal faults: Corrrespondence between three-dimensional mechanical models and field data. *Journal of Geophysical Research* **102,** 675–692.

Willemse, E. J. M. and Pollard, D. D. (1988) On the orientation and pattern of wing cracks and solution surfaces at the tips of a sliding flaw or fault. *Journal of Geophysical Research* (in press).

Yielding, G., Needham, T. and Jones, H. (1996) Sampling of fault populations using sub-surface data: a review. *Journal of Structural Geology* **18,** 135–146.